THE DARFIELD (CANTERBURY) EARTHQUAKE: GEODETIC OBSERVATIONS AND PRELIMINARY SOURCE MODEL

J. Beavan¹, S. Samsonov², M. Motagh³, L. Wallace¹, S. Ellis¹, N. Palmer¹

SUMMARY

High quality GPS and differential InSAR data have been collected for determining the ground deformation associated with the September 2010 Darfield (Canterbury) earthquake. We report preliminary results from a subset of these data and derive a preliminary source model for the earthquake. While the majority of moment release in the earthquake occurred on the strike-slip Greendale Fault a number of other fault segments were active during the earthquake including a steeply southeast-dipping thrust fault coincident with the earthquake hypocentre.

INTRODUCTION

The geological and seismological aspects of the Darfield earthquake are described elsewhere in this volume (Quigley et al., 2010; Gledhill et al., 2010). The earthquake occurred at 4:35 am local time on September 4th and caused surface rupture along the newly-recognised Greendale Fault. As indicated in Gledhill et al. (2010) and discussed further below, slip also occurred on a number of other buried fault segments during the earthquake. Following the earthquake we made immediate plans to reoccupy existing survey marks in the vicinity of the earthquake, and requested Japanese and European space agencies to collect satellite radar data over the region. The GPS surveys were carried out starting 3 days after the earthquake and the radar data were collected and processed as they became available. We report here on the geodetic data collected and on its processing to determine a preliminary source model for the earthquake. We also compare the ground level changes observed by GPS with those predicted by the

GEODETIC DATA

GPS data acquisition

We collected survey-mode GPS data in three stages. The sites we occupied are shown in Figure 1. In the first stage from September 7th – 13th we measured 80 sites within ~80 km of the earthquake in order to determine the coseismic (and a few days of postseismic) ground surface displacement field. We occupied a mix of sites that had high-quality pre-existing GPS observations within the past 2-3 years, and "3rd-order" sites with Land Information New Zealand (LINZ) Geodetic Database coordinates that had been calculated from GPS data collected more than 10 years ago. At the 25 "high-quality" stations we collected several 24-hour sessions of GPS data. At

the 55 "lower-quality" stations we collected at least one 24-hour session at five sites and one to several hours of data at the other 50. Seven of the latter stations were in the middle of roads, and data from these were collected using kinematic techniques with post-processing.

In the second stage from September 27th – 30th we reoccupied 45 of the sites closer to the earthquake and measured two additional sites, with sessions of at least 2 hours at the lower-quality sites and at least one session of 24 hours at five of the high quality stations. The intention was to see if a significant amount of postseismic displacement (afterslip or poroelastic effects) had taken place in the period between 1 and 3 weeks after the earthquake. We also measured longer sessions at three of the lower-quality stations in order to provide higher quality coordinates at these sites for future studies of longer-term postseismic deformation.

In the third stage from October $26^{th} - 29^{th}$ we occupied an additional 12 of the lower-quality sites with a 24-hour session, again to provide data for future post-seismic studies.

We also estimated the coseismic displacements recorded at stations in the GeoNet and LINZ continuous GPS (cGPS) networks. The largest displacement at a cGPS site was ~140 mm at McQueen's Valley (MQZG) south of Christchurch. Detectable displacements were observed at another 6 cGPS stations: Lyttelton (LYTT in Figure 1), Lake Taylor, Kaikoura, Westport, Hokitika and Waimate). A new LINZ cGPS station was scheduled to be installed by GeoNet near Methven (METH) in November. Due to the occurrence of the earthquake, GeoNet expedited this installation so that the station was recording data from September 11th.

In addition to the GNS-led GPS surveys, a survey commissioned by Christchurch City Council (CCC) was run on 9th September within Christchurch city and its immediate environs. We shared data with this survey and have

¹ GNS Science, Lower Hutt, New Zealand

² European Center for Geodynamics and Seismology, Walferdange, Grand Duchy of Luxembourg

³ GFZ, German Research Centre for Geosciences, 14473, Potsdam, Germany

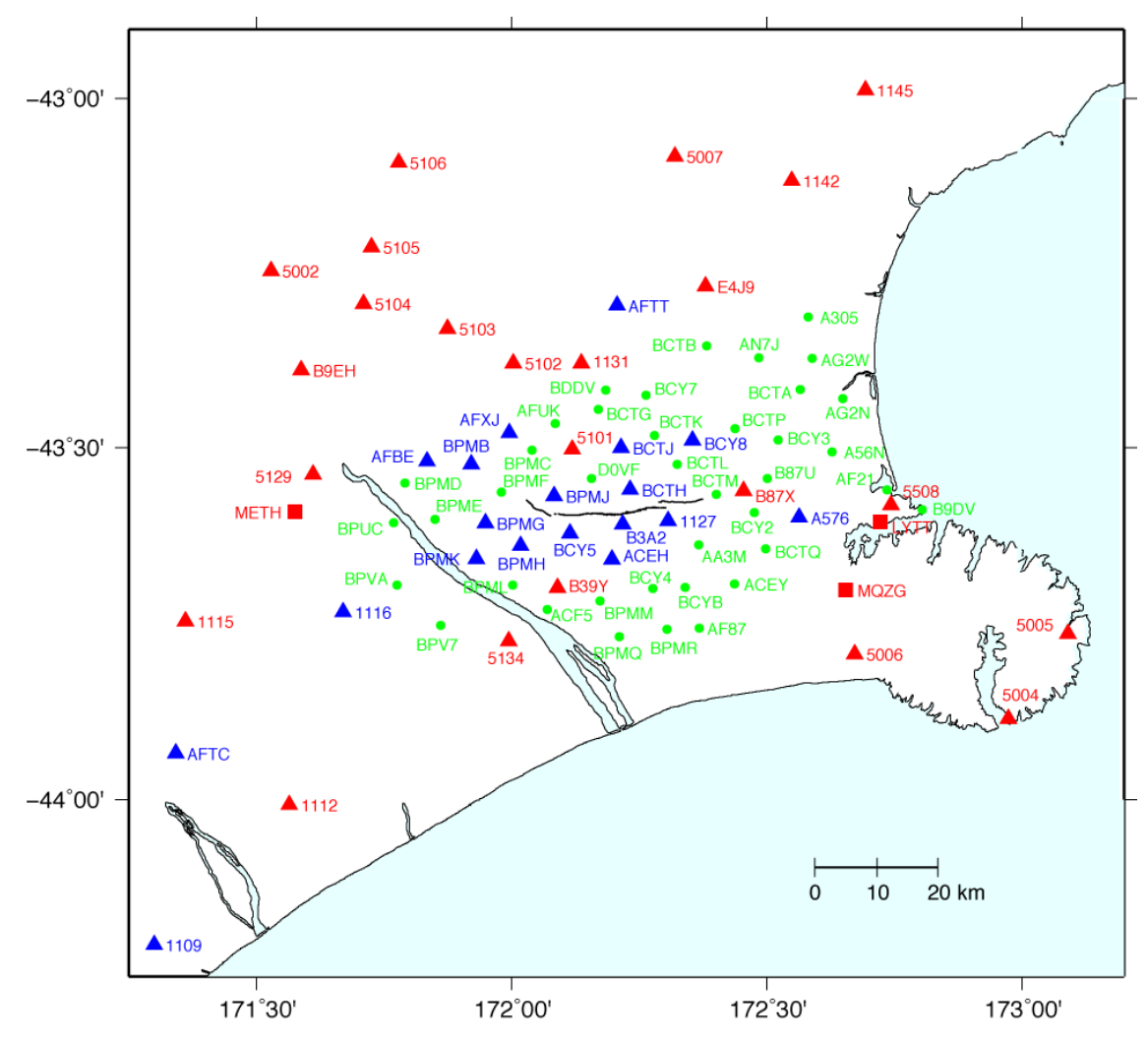


Figure 1: GPS sites occupied following the Darfield earthquake. Red squares show continuous sites (METH was installed 7 days after the earthquake). Red triangles show sites with high quality data both before and after the earthquake. Blue triangles have high quality data after the earthquake but lower quality data before. Green dots have lower quality data both before and after. Black line shows mapped surface rupture of the Greendale Fault. The earthquake epicentre is close to site D0VF.

incorporated some of the CCC data in our analysis. A survey has also been commissioned by LINZ, which concentrated on regions where GNS did not do high density surveys. The LINZ survey took place during October, and we have not so far incorporated these data into our processing.

GPS data processing

We processed the GPS data using standard techniques (e.g., Beavan et al., 2010) to provide post-earthquake coordinates for the sites. Because we only have the originally-calculated LINZ NZGD2000 coordinates for the lower-quality sites, we transformed the post-earthquake coordinates to their NZGD2000 values using transformation parameters calculated for LINZ by Beavan (2008). This transformation takes account of the ongoing plate boundary deformation and the difference in international terrestrial reference frames between the current frame (ITRF2005) and the one used for NZGD2000 (ITRF95). We then subtracted the two sets of NZGD2000 coordinates from each other to give the east, north and up displacements at these sites. We estimated the displacements at the high-quality stations by a similar method. We transformed both the post-earthquake coordinates and the most recent high-quality pre-earthquake coordinates to NZGD2000 and took their difference to give the estimated coseismic displacements. We assigned uncertainties to the displacements

based on whether they were estimated from two sets of lowquality coordinates, two sets of high-quality coordinates, or one of each. For the continuous GPS sites we estimated the displacements from the regionally-filtered GeoNet time series by averaging coordinates for several days before and after the earthquake and taking the difference. Figure 2a shows the GPS horizontal displacement vectors and Figure 2b the vertical displacements.

Differential InSAR data

We obtained a number of synthetic aperture radar images, using ALOS/PALSAR data from the Japanese Space Agency and Envisat data from the European Space Agency. We processed these using a variety of standard and advanced techniques to obtain differential interferometric synthetic aperture radar (DInSAR) images showing ground deformation in the line of sight from the ground to the satellite. We selected one image from each satellite for further processing. Both images are from ascending paths where the satellite is flying to the north-northwest and the radar is looking down and sideways towards the east-northeast (Figure 3). The ALOS radar beam has an incidence angle of 39° and the Envisat beam has an incidence angle of 23°, so the two satellites have a slightly different view of the ground displacement. Envisat is more sensitive to vertical deformation

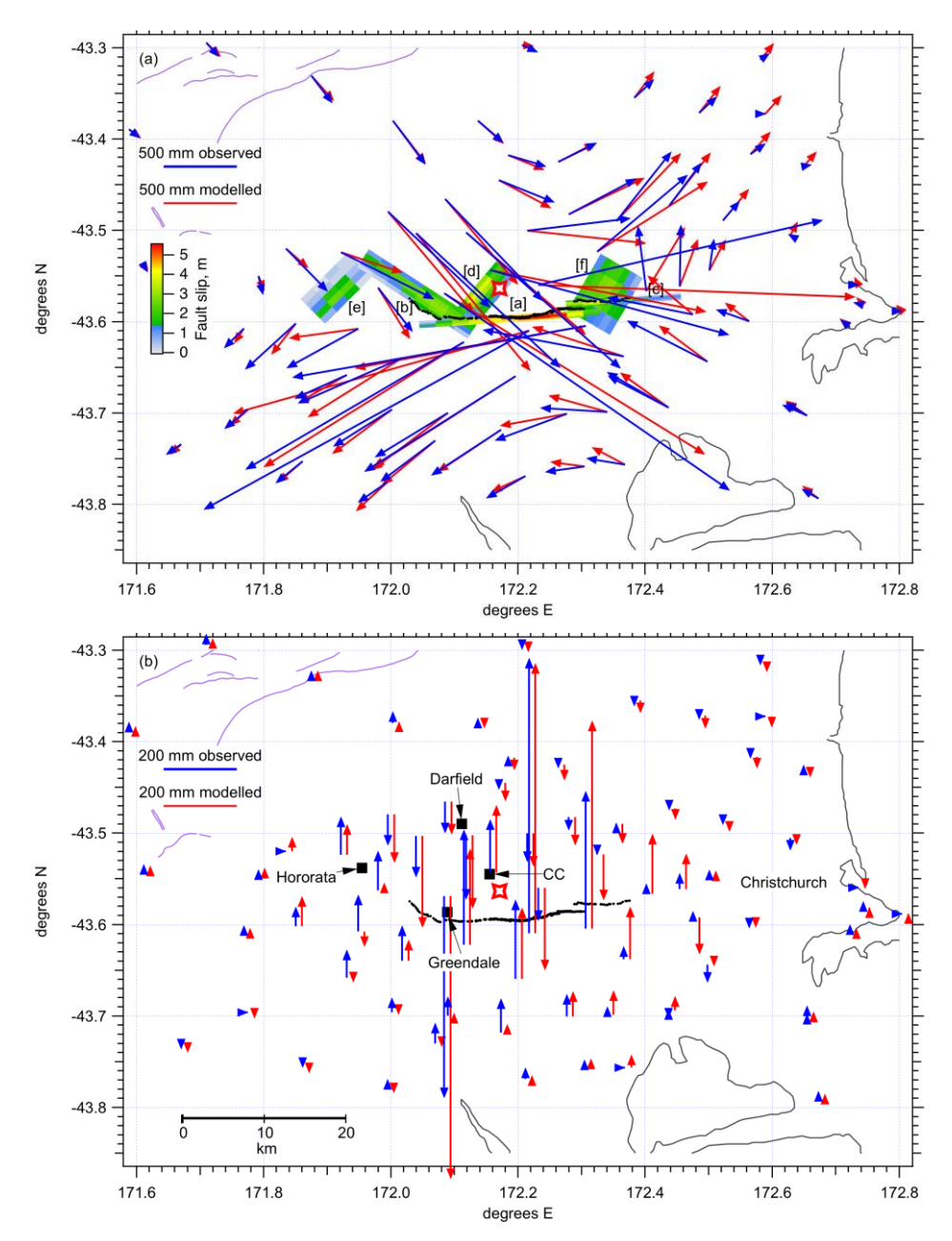


Figure 2: GPS observed (blue) and modelled (red) horizontal (a) and vertical (b) displacements. Red and white four-pointed star shows the epicentre. Black line shows the mapped surface rupture of the Greendale Fault. The coloured image in (a) shows the projection to the Earth's surface of the preliminary distributed slip model. The model consists of slip on the Greendale Fault plus three thrust segments on NE-oriented planes. In (a), letters [a] through [f] in square brackets are a cross-reference to the panels of Figure 6. The letters are located near the up-dip end of each fault segment. Place names referred to in the text are indicated by filled black squares in (b); CC is Charing Cross.

compared to horizontal by a factor of ~2.3, while for ALOS this factor is ~1.2. ALOS is therefore significantly more sensitive than Envisat to the horizontal component of ground motion. ALOS uses an L-band sensor with a wavelength of 236 mm and Envisat uses a C-band sensor with a wavelength of 56 mm. For ALOS the dates of the pre- and post-earthquake images are August 13th and September 28th. For Envisat they are September 1st and October 6th. In both cases the time difference is so short that corrections for interseismic displacement are unnecessary.

DInSAR images are interference patterns (or fringes) between two original radar images where each fringe, or cycle, represents ground displacement of half the radar wavelength along the line of sight from the ground to the satellite (e.g., Figure 3). The quality of the interferogram is described by coherence, which is the magnitude of the cross-correlation between two SAR images calculated in a small spatial window. The value of coherence ranges from zero (loss of coherence) to one (images are identical) and depends on a variety of parameters, including type of land-cover, length of spatial and temporal baselines between the two acquisitions, and radar wavelength. In general, images acquired by the longer wavelength sensor with small baselines over a low vegetation environment are the most coherent. The coherence also becomes low if the ground has been significantly disrupted, as it has been for example along the surface trace of the Greendale Fault. In order to obtain a surface displacement field for modelling, the interference fringes must be "unwrapped" by removing the fringe jumps. This procedure works well when the coherence between the images is high but can fail when the coherence is low. In regions of rapid displacement gradient this is a larger problem for C-band data

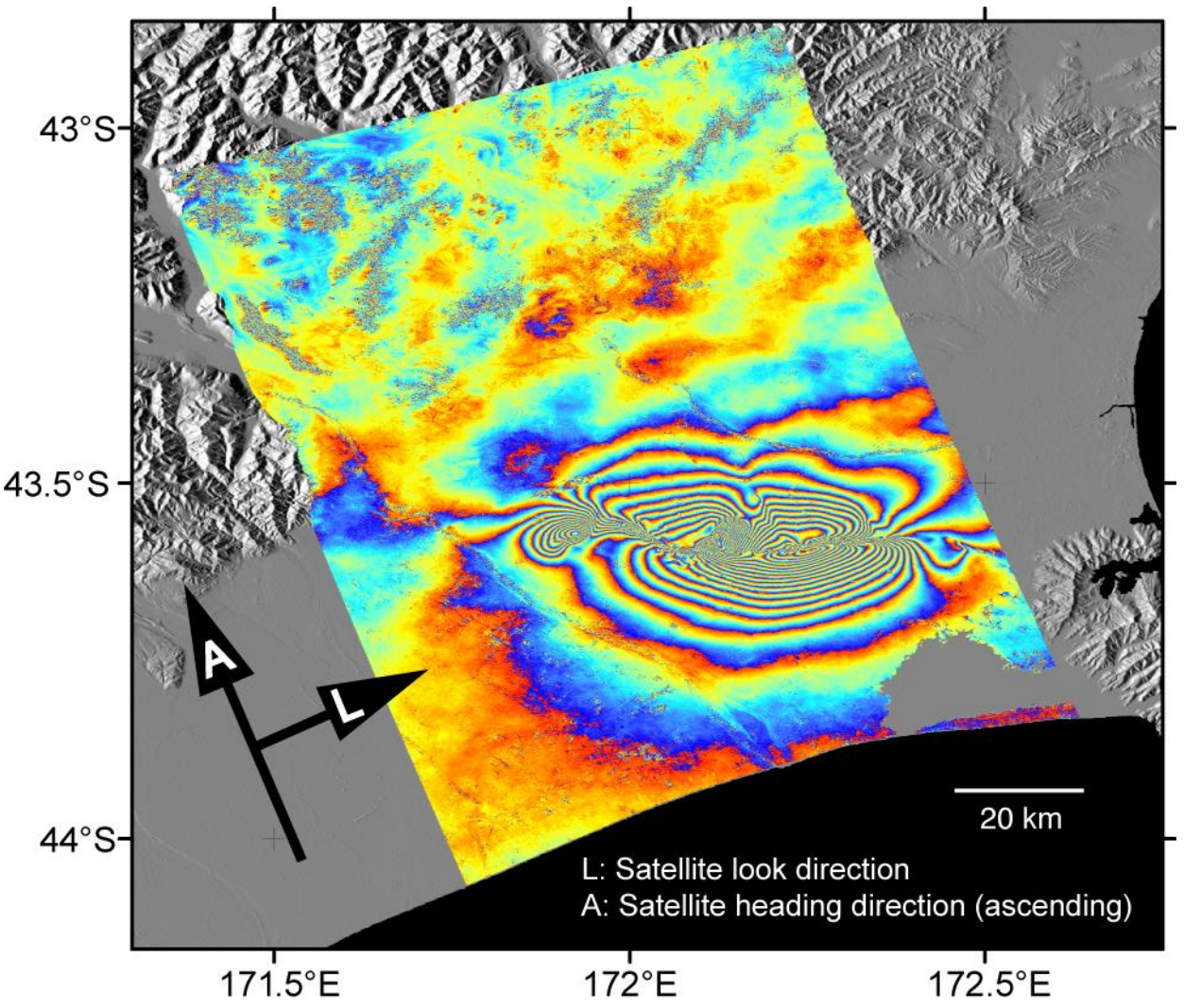


Figure 3: Original ALOS interferogram showing interference fringes that each represent 118 mm of ground motion in the line-of-sight to the satellite. The east-west and northwest-southeast strands of the Greendale Fault are clear in this image, as are the signatures of blind thrust faults near Charing Cross and Hororata. For the outer parts of the image it is clear that it is easy to unwrap the fringes to obtain the total ground displacement relative to the far field. This becomes progressively harder as the fringes get closer together (i.e., the displacement gradient increases) and as the coherence becomes lower. Regions of low coherence are concentrated along the Greendale Fault surface rupture and near the updip (northwest) end of the Charing Cross blind thrust on which the initial rupture occurred.

compared to L-band because of the shorter C-band wavelength. Unwrapping becomes impossible if displacements between adjacent pixels are larger than half the radar wavelength.

Figures 4a and 5a show the ALOS and Envisat observed interferograms after unwrapping, down-sampling and interpolation (see Beavan et al., 2010 for details of the method). The original data have been masked where the coherence is low, but in these down-sampled images there may be unwrapping and interpolation errors in the higherdeformation parts of the images (e.g., along the Greendale Fault trace). The main features of the images are the blue region to the north of the Greendale Fault which indicates motion away from the satellite (i.e., generally eastward or downward ground displacement) and the red region to its south indicating motion towards the satellite (i.e., generally westward or upward ground displacement). This pattern is as expected for an east-west right-lateral strike-slip fault. The northeast-southwest oriented region of green (essentially no displacement in the direction towards the satellite) that interrupts the blue region to the northeast of the bend in the Greendale Fault is highly indicative of an additional eastward or southeastward dipping thrust fault in this region that causes

ground surface displacement towards the satellite that approximately cancels the away displacement due to the strike-slip fault. The ALOS signal (Figure 4a) has a greater amplitude than the Envisat signal (Figure 5a) because of the higher sensitivity of ALOS to horizontal motion.

MODELLING

We first inverted the GPS displacement data using a model consisting of uniform slip on several rectangular fault planes. The inversion software uses a non-linear least-squares method (Darby & Beavan, 2001) to solve for all nine parameters of each fault, though some parameters had to be fixed to keep the solution stable. The GPS data require at least three faults to be active during the earthquake: the largely right-lateral Greendale Fault and its buried extension for several km beyond the northwest end of the currently-mapped surface rupture; a blind thrust coincident with the earthquake hypocentre; and a blind thrust at the northwest end of the strike-slip fault near Hororata (see Figure 2b for location).

We then jointly inverted the GPS and DInSAR data using linear least-squares inversion software in which the fault planes are pre-defined, and solving for the variable slip on

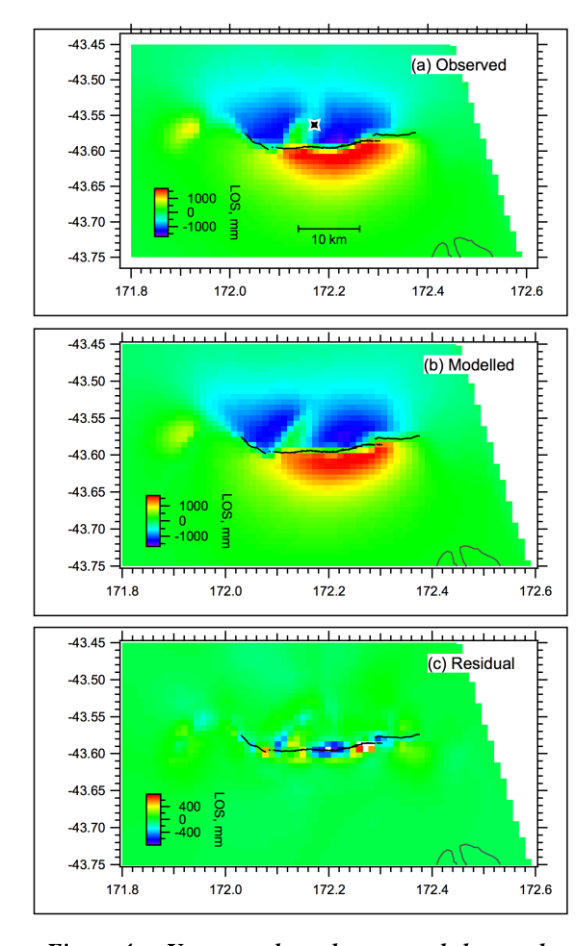


Figure 4: Unwrapped, down-sampled and interpolated Aug 13–Sep 28 ALOS interferogram (a) observed; (b) modelled; (c) residual. Note change of scale in (c). The black line shows the mapped surface rupture of the Greendale Fault. The four-pointed star in (a) shows the epicentre.

each fault plane. This is a standard method with an implementation recently described by Beavan *et al.* (2010). We have adapted the method to solve for slip on several fault planes rather than a single fault surface. We begin by using the planes determined in the GPS solution then modify the locations, strikes and dips of these planes in order to reduce the residuals between the observations and the model fits. We also add additional planes where this is indicated by significant residuals in the DInSAR images.

Our preliminary solution consists of the Greendale Fault, a blind thrust between Greendale and Charing Cross that we call the Charing Cross thrust for the purposes of this paper, and a blind thrust near Hororata. As well as these, at least two additional fault segments are required towards the eastern end of the rupture to fit the GPS and DInSAR observations. We include one of these faults in the solution reported here as its inclusion substantially reduces both the GPS and DInSAR residuals. We approximate the Greendale Fault as three planar segments — the main east-west rupture, the northwest-southeast striking segment to its west and the offset-to-thenorth east-west section to its east (planes [a] through [c] in Figure 2).

The modelled DInSAR data and the residuals (observed-modelled) are shown in Figures 4b, 4c, 5b and 5c, while the observed and modelled GPS data are shown in Figure 2.

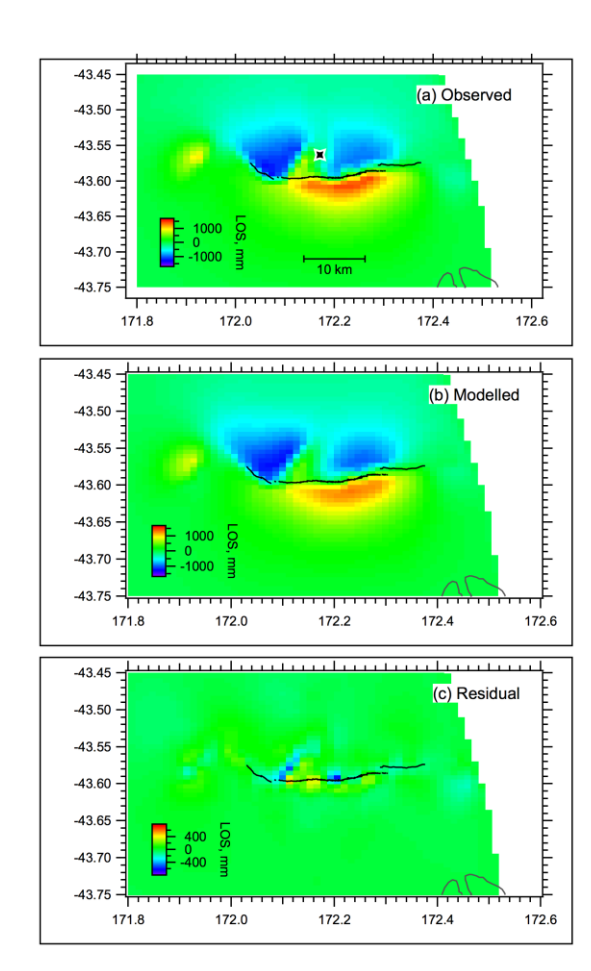


Figure 5: Unwrapped, down-sampled and interpolated Sep 1-Oct 6 Envisat interferogram (a) observed; (b) modelled; (c) residual. Note change of scale in (c). The black line shows the mapped surface rupture of the Greendale Fault. The four-pointed star in (a) shows the epicentre.

The inferred slip distribution on each fault plane is shown in Figure 6. The displacements are plotted for the hanging wall relative to the footwall. For the Greendale Fault the central and eastern sections dip steeply to the south so these slip distributions are viewed from the south. However, the western section dips to the northeast, so this slip distribution is viewed from the northeast. For the blind thrust segments the Charing Cross thrust dips to the southeast, while the thrust near Hororata dips to the northwest in agreement with interpretations of seismic reflection data (Forsyth et al., 2008; R. Jongens, pers. comm.). The horizontal scale shows the distance along strike from the left end of the fault as viewed from the hanging wall. The vertical scale shows the distance down dip from the surface. The strike-slip faults are modelled from the surface downwards, whereas the top edges of the thrust faults are sub-surface.

The moment magnitude (M_W) for each fault plane in the model is calculated by summing area \times slip magnitude over the cells in that plane and multiplying by an assumed rigidity of 3×10^{10} Nm to give the moment (M_0) , then applying the standard relationship $M_W = 2/3 \times \log_{10}(M_0) - 6.03$.

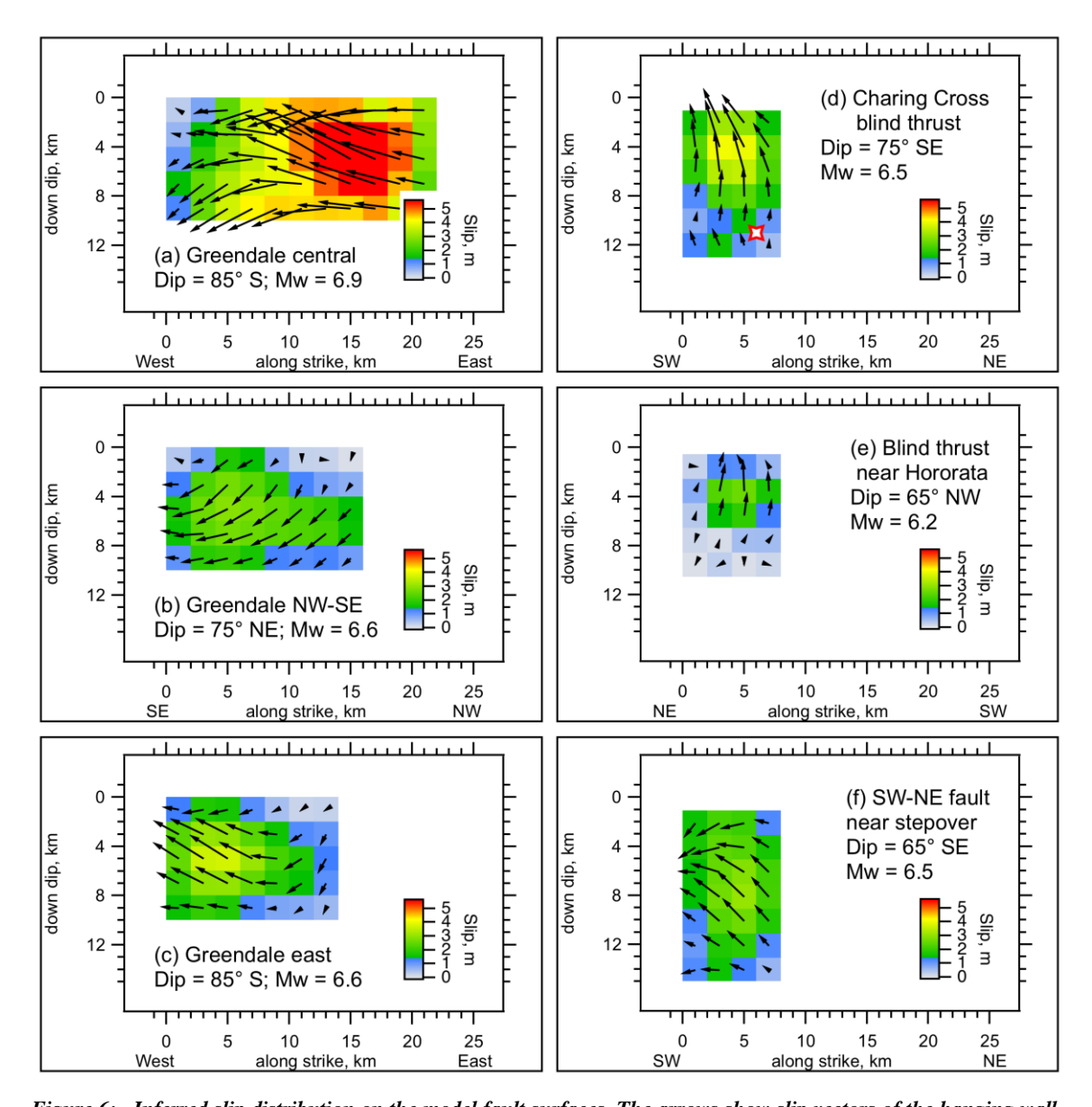


Figure 6: Inferred slip distribution on the model fault surfaces. The arrows show slip vectors of the hanging wall relative to the footwall. The coloured image gives the slip magnitude. The red-and-white star in (d) shows the GeoNet location of the hypocentre, which is coincident with the model fault plane. The Greendale Fault is modelled as three separate segments (a)-(c). The geographic locations of the fault segments are indicated on Figure 2. The bottom axes show the distance along strike from the left-hand end of the fault segment as viewed from the hanging wall. The left axes show the distance down dip measured from the surface. The length of the Greendale Fault rupture is ~40 km if the sections at the northwestern and eastern ends that did not rupture to the surface are included.

DISCUSSION

Source Model

We assume the blind thrust between Charing Cross and Greendale to be the source of the initial rupture because the plane coincides with the earthquake hypocentre and because the inferred strike, dip and slip direction are in close agreement with the seismologically-determined first-motion and regional-CMT focal mechanism solutions (Gledhill *et al.*, 2010). Though the thrust initiated at 11 km depth, the maximum slip was centred at about 4 km depth (Figure 6d). The order in which the other fault segments failed cannot be determined from the geodetic data, which only provide the total displacement during the coseismic event and the first few days of postseismic deformation. However, it seems likely that the Charing Cross thrust triggered rupture on the Greendale

Fault that propagated both east towards Christchurch and northwest towards Hororata. Analysis of strong motion records should allow both the slip distribution and the timing of the rupture to be accurately determined (C. Holden, pers. comm.; Cousins & McVerry, 2010).

The seismic moment for the Greendale Fault (adding the three segments together) is $M_W=7.0$. The majority of moment release is on the central section (Figure 6a). Buried slip continues both to the northwest of the mapped rupture at the western end of the fault (> 2 m slip for 6-7 km additional distance) and to the east of its eastern end (> 2 m slip for 2-4 km). The northwestern segment (Figure 6b) has a significant component of normal slip down to the northeast. The rupture of this segment towards the northwest could have triggered the failure of the blind thrust near Hororata. The modelled slip at the surface (Figures 6a-6c) appears to agree well with the mapped surface rupture displacements in terms of both magnitude and distribution, though a detailed comparison has

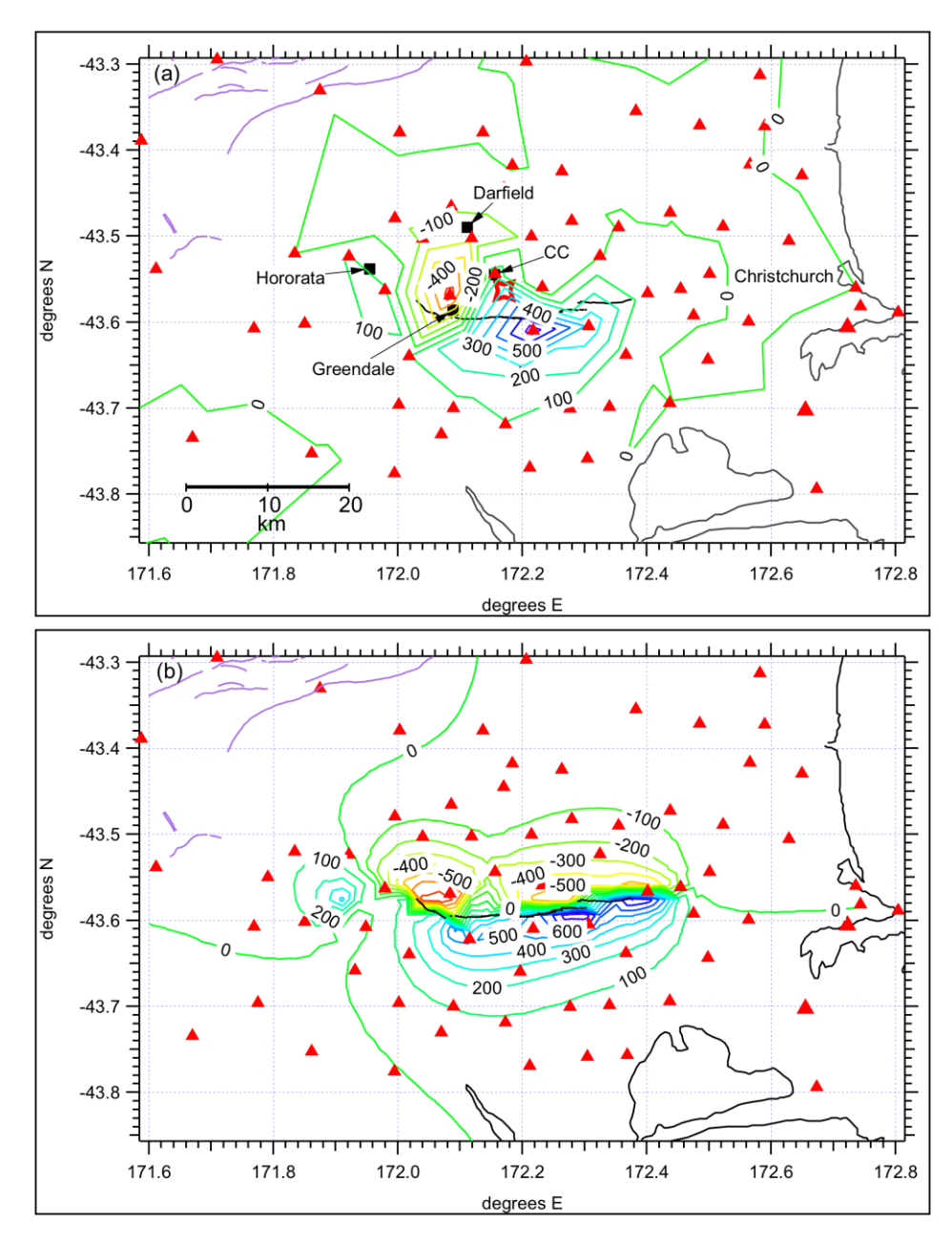


Figure 7: Land level changes in mm contoured from (a) GPS vertical displacement observations and (b) calculated vertical displacements using the preliminary earthquake source model. The GPS observation points are shown as red triangles and the Greendale Fault surface rupture is plotted as a black line. A number of features of the vertical displacement field are not detected by the observed GPS data alone. The inclusion of DInSAR data in the model allows these features to be delineated.

not yet been made. The length of the Greendale Fault is ~40 km if the sections of significant slip at the northwestern and eastern ends that did not rupture to the surface are included. Interestingly, the blind thrust fault imaged geodetically near Hororata is given additional credence by field observations of stretched fences and minor road cracking coincident with the model thrust (D. Barrell, pers. comm.; Quigley *et al.*, 2010).

After including the Greendale Fault, the Charing Cross thrust (Figure 6d) and the thrust near Hororata (Figure 6e) in the model, significant residuals remain in both the GPS and DInSAR data, especially towards the eastern end of the rupture. A region of ground displacement towards the satellite occurs both north and south of the Greendale Fault near the stepover. This can be modelled by an additional SW-NE trending fault segment in this region, with similar geometry to the Charing Cross thrust. We have included this fault in the model (Figure 6f) as it significantly reduces the residuals between modelled and observed displacements. A region of

motion away from the satellite southeast of the eastern end of the Greendale Fault (seen most clearly as a blue region near the right edge of the image in Figure 5c) will require another fault segment. There are many aftershocks in this region, but so far they have only been routinely located so there is no useful depth control that may help to define active fault planes. Work is ongoing to relocate the aftershocks with a 3-D velocity model (M. Reyners, pers. comm.).

The postseismic deformation is small, with the largest reliably-determined GPS displacements in the period from 1 to 8 weeks after the earthquake being 10 mm or smaller, on the order of 1% of the coseismic displacement. This implies that the great majority of the ground deformation occurred at the time of the earthquake, so that we are not introducing significant error by using GPS and DInSAR data collected days to weeks after the event.

There are significant residuals remaining between the observed and modelled ground displacements, especially along the Greendale Fault and in the region of the Charing Cross thrust. These could result from a variety of sources, including the model fault not accurately following the mapped rupture and unwrapping errors due to low coherence. Additional work is required to address these issues.

The complexity of the rupture is reminiscent of the 1994 Arthurs Pass earthquake, which also included a strike-slip segment (Arnadottir *et al.*, 1995; Abercrombie *et al.*, 2000) with several cross-faults delineated by aftershocks (Bannister *et al.*, 2006). The Darfield event is vastly better documented, which should in time enable us to learn much more about the reasons for the complexity.

Vertical deformation

The land level changes caused by the earthquake are of significant engineering and hydrological interest, with the diversion of the Hororata River (Figure 4 of Quigley *et al.*, 2010) being one of the larger-scale effects. We plot level changes as contoured from the observed GPS vertical displacements in Figure 7a, and as calculated using the preliminary source model in Figure 7b. The main features in the observed contours are the ~550 mm subsidence near Greendale and the ~750 mm uplift south of the Greendale Fault. There is minor subsidence (excluding the effects of slumping and liquefaction) of less than ~50 mm throughout Christchurch City as was also confirmed by the more detailed CCC survey (K. Blue, pers. comm.).

The model contours show the same large uplift and subsidence features close to the fault, but with an increase in detail. They also show other features where the GPS station spacing was insufficient to capture the signal. The clearest of these is the 400 mm uplift southwest of Hororata caused by the shallow blind thrust in this area (Figure 6e), which is only hinted at in the GPS vertical observations; the GPS sites neatly surround the uplift zone but there are no sites actually within it. This is an example of the advantage provided by using the high spatial density DInSAR observations in addition to the GPS. We are aware of additional vertical deformation datasets along parts of the fault (B. Duffy, pers. comm.; D. Tombleson, pers. comm.) and these can be used in the future to verify the accuracy of the model in these areas.

CONCLUSIONS

We have derived a preliminary source model for the Darfield earthquake based on geodetic data collected before and after the earthquake and have used it to produce a contour map of land level changes. The source shows considerable complexity with several northeast-striking thrust faults active in addition to the main, largely right-lateral strike-slip, failure on the Greendale Fault. The estimated moment magnitudes for the Greendale Fault and the Charing Cross thrust fault on which the rupture initiated are $M_W = 7.0$ and $M_W = 6.5$ respectively. The moment magnitude including all modelled fault segments is $M_W = 7.1$. While we stress that this is a preliminary model that will be improved with further work and additional data, we believe that the main features of the model are robust.

ACKNOWLEDGEMENTS

We thank Dave Collett, Josh Thomas, Kelvin Tait (all at LINZ), Joe Wright (Otago University), Kirby MacLeod, Charles Williams (both at GNS), Richard Davy and Adam Carrizales (both at Victoria University) for their contributions to the GPS surveys. We thank Nicola Litchfield and Biljana Lukovic for providing the Greendale Fault coordinates, Simon Cox for suggesting the inclusion of the section on vertical

deformation, and Russ Van Dissen, Caroline Holden, Mark Quigley and David Barrell for their reviews and suggestions on the manuscript. Envisat data were provided by the European Space Agency (ESA) under the Cat-1 proposal AOALO3740. We have used ALOS data that is © Japan Aerospace Exploration Agency ("JAXA") and the Japanese Ministry of Economy, Trade and Industry ("METI") (2010). The data has been used with the permission of JAXA and METI and the Commonwealth of Australia (Geoscience Australia) ("the Commonwealth"). JAXA, METI and the Commonwealth have not evaluated the data as altered and incorporated in this paper, and therefore give no warranty regarding its accuracy, completeness, currency or suitability for any particular purpose.

REFERENCES

- Abercrombie, R.E., Webb, T.H., Robinson, R., McGinty, P.J., Mori, J.J., Beavan, R.J. (2000), "The enigma of the Arthur's Pass, New Zealand, earthquake 1: Reconciling a variety of data for an unusual earthquake sequence". *J. Geophys. Res.* **105**: 16,119-16,137.
- Arnadottir, T., Beavan, J., Pearson, C. (1995), "Deformation associated with the 18 June 1994, Arthur's Pass earthquake, New Zealand. N. Z. J. Geol. Geophys. 38: 553-558.
- Bannister, S., Thurber, C., Louie, J. (2006), "Detailed fault structure highlighted by finely relocated aftershocks, Arthur's Pass, New Zealand". *Geophys. Res. Lett.* **33:** L18315. doi:10.1029/2006GL027462
- Beavan, J. (2008), "Consultancy services for PositioNZonLine, Phase 2 (PONL-02)". GNS Science Consultancy Report 2008/136: 79 p. GNS Science, Lower Hutt, New Zealand.
- Beavan, J., Samsonov, S., Denys, P., Sutherland, R., Palmer, N., Denham, M. (2010), "Oblique slip on the Puysegur subduction interface in the July 2009 M_W 7.8 Dusky Sound earthquake from GPS and InSAR observations: implications for the tectonics of southwestern New Zealand". Geophys. J. Int. doi: 10.1111/j.1365-246X.2010.04798.x
- Cousins, J., McVerry, G. (2010), "Overview of strong motion data from the Darfield Earthquake". *Bulletin of the New Zealand Society for Earthquake Engineering* **43:** this volume.
- Darby, D.J., Beavan, J. (2001), "Evidence from GPS measurements for contemporary plate coupling on the southern Hikurangi subduction thrust and partitioning of strain in the upper plate". J. Geophys. Res. 106: 30,881-30,891.
- Forsyth, P.J., Barrell, D.J.A., Jongens, R. (2008), "Geology of the Christchurch area". Institute of Geological and Nuclear Sciences 1:250,000 Geological Map 16. 1 sheet + 67 p. GNS Science, Lower Hutt, New Zealand.
- Gledhill, K., Ristau, J., Reyners, M., Fry, B., Holden, C., and the GeoNet Team (2010), "The Darfield (Canterbury) earthquake of September 2010: Preliminary seismological report". *Bulletin of the New Zealand Society for Earthquake Engineering* **43**(4): this volume.
- Quigley, M., Van Dissen, R., Villamor, P., and 20 others (2010), "Surface rupture of the Greendale Fault during the Darfield (Canterbury) earthquake, New Zealand: Initial findings". Bulletin of the New Zealand Society for Earthquake Engineering 43(4): this volume.